Modification of natural clinoptilolite zeolite to enhance its hydrogen adsorption capacity

Sema Akyalcin[1] [ORCID] · **Levent Akyalcin[1]** [ORCID] · **Ecem Ertugrul[1]** [ORCID]

Abstract

In this study, natural clinoptilolite was treated with HCl, HNO_3, and $C_2H_2O_4$ at various concentrations (0.1, 0.5, and 1.0 M) at different temperatures (60, 70, and 80 °C) and treatment times (2, 3, and 4 h). The hydrogen adsorption capacity of natural clinoptilolite increased from 0.446 to 3.255 mmol/g after treating with 0.5 M HNO_3 at 80 °C for 2 h. The correlation of the newly produced textural and structural properties with hydrogen adsorption ability is explained by characterizing the modified clinoptilolites using X-ray fluorescence (XRF), X-ray diffraction (XRD), nitrogen adsorption/desorption isotherms, and temperature programmed desorption of ammonia (NH_3-TPD) measurements. The results show that the hydrogen adsorption capacity of modified clinoptilolites is associated with both the quantity and strength of the strong acid sites, in addition to the enhanced surface area and micropore volume. The hydrogen adsorption data for natural and acid-treated clinoptilolite samples at 77 K obeyed the Freundlich isotherm model.

Keywords Natural zeolite · Clinoptilolite · Acid treatment · Hydrogen adsorption · Adsorption isotherm

Introduction

The world is grappling with the challenges caused by climate change and is attempting to reduce greenhouse gas emissions. Carbon dioxide (CO_2) emissions constitute 75% of the global greenhouse gas emissions. Furthermore, the contribution of transportation to total greenhouse gas emissions is 23%, 70% of which is due to the fossil

✉ Levent Akyalcin
lakyalcin@eskisehir.edu.tr

Sema Akyalcin
sdogruel@eskisehir.edu.tr

Ecem Ertugrul
ecemmertugrul@gmail.com

[1] Department of Chemical Engineering, Eskişehir Technical University, 26555 Eskişehir, Turkey

fuels used by road vehicles [1, 2]. Since the 1960s, the replacement of the internal combustion engine used in road vehicles with more effective, low-emission alternative power sources has been discussed, and it has been contended that fuel cells are the power source that most closely matches the internal combustion engine. Currently, there is still much support for this viewpoint [3]. Based on this view, many countries are concentrating on hydrogen to reduce their carbon emissions and their dependency on fossil fuels, and to use it in fuel cells as an energy source [4, 5].

Hydrogen is a simple molecule with the lowest energy density per unit of volume. However, the energy density per unit weight was higher than that of the other fuels. For this reason, hydrogen is used as a fuel in energy conversion systems, such as fuel cells. Hydrogen undergoes oxidation in a fuel cell, resulting in the production of power and water. Consequently, the process does not release any greenhouse gases, unlike fossil fuel combustion, and is thus not detrimental to the environment. Moreover, the calorific value of hydrogen is three times higher than petroleum [6]. Although hydrogen is an expensive fuel owing to its production cost, hydrogen generation is possible using different primary energy sources [7].

The critical link between hydrogen generation and its use as a clean energy source for transportation is hydrogen storage. Four different methods were used for hydrogen storage. These include i) gas under high pressure, ii) liquid hydrogen, iii) chemical adsorption, and iv) physical adsorption. For hydrogen storage as a gas under high pressure, steel or aluminum containers alone are insufficient in terms of mechanical strength, and composite containers with high mechanical strength, in which carbon fiber and resin are also used, are being developed. However, the cost and maintenance of these containers are barriers to the use of hydrogen-using fuel cells. More liquefied hydrogen can be stored per unit volume than high-pressure hydrogen gas. This storage method has a higher storage density than the other methods. However, the energy cost required to liquefy hydrogen is high and hydrogen evaporates at room temperature, causing losses. The need for cryogenic temperature requires liquid-hydrogen containers to be thermally insulated. As a result, cryogenic hydrogen containers typically employ vacuum insulation; these are vessels consisting of two walls with a vacuum in between them to provide thermal insulation. This approach reduces heat loss and improves storage efficiency. However, boiling losses are expected to occur due to thermal conduction through other components, while heat flows from the medium to liquid-hydrogen [8]. The chemisorption method was used to store hydrogen in the gas phase of solid metal hydrides. Many metal-hydride materials have been used for this purpose. Although metal hydrides have a high storage capacity, low cost, and lightweight, high temperatures are required to release hydrogen from the metal hydride structure because hydrogen molecules are strongly bound in the metal hydride structure and have slow reaction kinetics. Physisorption deposition is the weak adsorption of hydrogen molecules on the material surface by London dispersion forces. It is attractive in terms of cost because it can store hydrogen molecules at room temperature and relatively low pressure using physisorption technology. The materials used in physisorption are generally porous because a large surface area is required. The advantages of this method include its light weight, high storage density, superior reversibility, cycle stability, and fast charging–discharging rate. Zeolites, metal–organic frameworks (MOFs), covalent organic frameworks

(COFs), and carbon materials are considered to be physisorption materials. Each of these materials exhibits characteristics such as shape selectivity, adsorption capacity, stability, and durability [9].

Zeolites are highly crystalline alumina silicate materials that can be synthesized industrially or mined naturally. Owing to their lattice and channel structures, high thermal stability, and large ion exchange capacities, they have outstanding potential for encapsulating nonpolar gases such as hydrogen [10]. Zeolites with a high Si/Al ratio and high hydrophobicity exhibit strong interactions with nonpolar molecules [11]. The zeolites with different Si/Al ratios can be obtained via hydrothermal synthesis or post-synthesis methods. However, the post-synthesis method is applicable to arrange SiO_2/Al_2O_3 ratios for the natural zeolites, which is carried out by dealuminating of the zeolites using acid treatment or desilicating of the zeolites using alkali treatment. The acid treatment could remove part of aluminum from framework of natural zeolite and the corresponding SiO_2/Al_2O_3 ratios of zeolites increased based on the dealumination efficiency of acid treatment [11]. Wang et al. stated that the acid-treated zeolites with different Si/Al ratios controlled by acid concentration had higher specific surface area, micropore volume, silanol group content, and hydrophobicity than those for the natural zeolites [11].

Clinoptilolite is a low-cost, abundant natural zeolite. It has a two-dimensional channel system and consists of two parallel channels forming from a 10-membered ring (7.2 Å × 4.4 Å) and an 8-membered ring (4.7 Å × 4.1 Å) that intersect with a third channel composed of 8- membered rings (5.5 Å × 4.0 Å) [12, 13]. The framework of clinoptilolite is composed of SiO_4 and AlO_4 tetrahedra with charge-balancing cations, such as Na^+, K^+, Ca^{2+}, and Mg^{2+}. The presence of cations or minerals in the zeolite structure affects its adsorption capacity, and acid treatment causes decationization and dealumination, rendering an improved adsorbent from natural zeolite [14]. The type, location, and distribution of exchangeable cations and the corresponding effects of these cations on channel blockage affect the adsorption and diffusion of modified clinoptilolite [15, 16].

There are a limited number of studies on hydrogen adsorption on natural clinoptilolite [17, 18]. Erdoğan and Dikmen investigated the effects of acid type (HCl, HNO_3, and H_2SO_4) and acid concentration (2.0, 4.0, and 6.0 M) on clinoptilolite-rich tuff at 90 °C for 4 h. They state that the hydrogen adsorption capacities of the prepared samples are between 1.609 and 2.391 mmol/g, and the hydrogen adsorption capacities of these samples were decreased, although significant increases in microporous surface areas and micropore volumes with the nitric and hydrochloric acid treatments up to 4.0 M [18].

Acid treatment can affect the physicochemical features of natural zeolites and improve their hydrogen adsorption capacity. The effective parameters in acid treatment are the acid type, concentration, operating temperature, and time [19]. Therefore, the optimal acid treatment conditions to enhance the hydrogen adsorption capacity of natural zeolites must be determined.

The Taguchi method is an effective experimental methodology that focuses on minimizing the number of experiments needed within a certain range of factors and levels. It involves designing experiments, analyzing the signal-to-noise (S/N) ratio, and optimizing the results. The method uses orthogonal arrays to efficiently identify

significant factors, assess each experiment's performance, and determine the optimal levels of factors for optimal performance [20–22].

This study aimed to develop an economical and effective method for producing H_2 storage materials from natural zeolites and determine the relationship between the physicochemical properties and hydrogen storage capacity of modified zeolites. Natural clinoptilolite, which is widely distributed and economically mined worldwide, was selected as the hydrogen-adsorption material. The Taguchi method was used to improve the acid treatment parameters of natural clinoptilolite to maximize its hydrogen adsorption capacity. The correlation between the newly produced textural and structural properties and the hydrogen storage performance of the modified clinoptilolite samples is discussed.

Experimental

Materials and preparation of natural clinoptilolite

Hydrochloric acid (HCl, 37%, extra pure), nitric acid (HNO_3, 65%, Emsure grade), and oxalic acid dihydrate ($C_2H_2O_4 \cdot 2H_2O, \geq 99.0\%$) were purchased from Merck. Hydrogen gas (N5.5 purity) and nitrogen gas (N5.0 purity) were provided by Linde.

The natural clinoptilolite Gördeş (Manisa, Türkiye) was supplied by Rota Mining Corporation in powder form with a particle size of 10 μm. Initially, 25 g of raw samples were washed with 500 mL of deionized water at 50 °C for 2 h to remove the soluble salts and then dried in an oven at 80 °C overnight. The natural form of the clinoptilolite sample was labeled S0 and stored in a desiccator.

Modification of natural clinoptilolite

An experimental design with four factors and three levels of each factor was used to modify the S0 clinoptilolite sample (Table 1). The factors are the acid solution (HCl, HNO_3, and $C_2H_2O_4$), concentration of the acid solution (0.1, 0.5, and 1.0 M), treatment temperature (60, 70, and 80 °C), and treatment time (2, 3, and 4 h). The treated samples, filtered from the solution, were then rinsed with deionized water to neutralize them before being dried in an oven for 16 h at 80 °C.

Table 1 Experimental parameters and their levels

Symbol	Parameters	Levels		
		1	2	3
A	Concentration of solution, M	0.1	0.5	1.0
B	Type of solution	HCl	HNO_3	$C_2H_2O_4$
C	Temperature, °C	60	70	80
D	Time, h	2	3	4

Orthogonal array and experimental parameters

Taguchi's experimental design method was used to determine the best clinoptilolite modification characteristics for hydrogen adsorption. The Taguchi approach uses an orthogonal array (OA) to conduct experiments and evaluate the results by calculating the signal-to-noise ratio (S/N). Based on the number of parameters and their levels in Table 1, the L9 orthogonal array design in Table 2 was selected [22]. This study aimed to improve the ability of clinoptilolite samples to adsorb hydrogen; as a result, the larger-the-better hydrogen adsorption capacity of the sample was designated as the performance characteristic.

Characterization and hydrogen adsorption of clinoptilolite samples

The chemical compositions of the natural and modified clinoptilolite samples were measured using wavelength-dispersive X-ray fluorescence spectroscopy (WD-XRF) with a Rigaku ZSX-Primus. The crystal structures of the clinoptilolite samples were determined by X-ray diffraction (XRD, Rigaku MiniFlex 600). The measurements were obtained in the range of (2θ) 5°to 40° at a scan rate of 0.02°/s using CuKα radiation ($\lambda = 0.15406$ nm).

The acidity of the natural and modified clinoptilolite samples was analyzed by temperature-programmed desorption of ammonia (NH$_3$-TPD) measurements performed on a Quantachrome Autosorb IQ-Chemi-XR instrument. For NH$_3$-TPD analysis, approximately 100 mg of the sample was flushed with 50 mL/min of helium stream for 3 h at 350 °C, then cooled to 100 °C and saturated with pure ammonia flow at 100 °C for 30 min. The sample was then flushed with 50 mL/min of helium stream for 2.5 h to remove loosely adsorbed NH$_3$, and the remaining strongly adsorbed NH$_3$ was desorbed by increasing the temperature to 700 °C at a heating rate of 10 °C/min.

A Quantachrome Autosorb IQ-MP-XR instrument was used to obtain the hydrogen and nitrogen adsorption isotherms of the natural and modified clinoptilolite samples at 77 K. Samples were outgassed for 12 h at 300 °C in vacuum before the measurement. The size distributions of the unmodified and modified clinoptilolite

Table 2 L$_9$ orthogonal array layout

Experiment no	A	B	C	D	Sample no
1	1	1	1	1	S1
2	1	2	2	2	S2
3	1	3	3	3	S3
4	2	1	2	3	S4
5	2	2	3	1	S5
6	2	3	1	2	S6
7	3	1	3	2	S7
8	3	2	1	3	S8
9	3	3	2	1	S9

samples were estimated using the nonlocal density functional theory (NLDFT) technique. The kernel was "N$_2$ at 77 K on silica, cylindrical pores, and adsorption branches " for the NLDFT [23].

Results and discussion

Characterization of clinoptilolite samples

The bulk chemical compositions of the natural (S0) and modified clinoptilolites (S1-S9) are listed in Table 3.

XRF analysis shows the contents of Si, Al, Na, K, Mg, Ca, Fe, Ti, and Mn in the natural clinoptilolite crystal. Table 3 indicates that the S0 sample had high potassium and calcium contents, whereas the sodium and magnesium contents were low. The most common charge-balancing cations of clinoptilolite are Na$^+$, K$^+$, Mg^{2+}, and Ca^{2+} [15]; thus, the presence of Fe, Ti, and Mn can be considered to be impurities of the clinoptilolite originating from the zeolitic tuff. Moreover, it was observed that the acid treatment expelled Na$^+$ and Mg^{2+} cations from the framework (S1-S9). As the acid concentration increased from 0.1 M to 1.0 M, the concentrations of K, Ca, and Fe atoms decreased progressively (S1-S9). While the CaO concentration was mainly reduced in the HCl treatment (S1, S4, S7), the K$_2$O and Fe$_2$O$_3$ contents significantly decreased in the oxalic acid treatment (S3, S6, S9). The treatment of natural clinoptilolite with an increasing concentration of oxalic acid solution increased the Si/Al molar ratio owing to dealumination (S3, S6, S9). XRF data confirmed that the acid treatment conditions changed the composition of the natural clinoptilolite.

The XRD patterns of the natural and modified clinoptilolite samples are shown in Fig. 1. The diffraction peaks observed at 2θ values of 9.88°, 11.24°, 22.42°, 26.06°, 28.18°, 30.12°, and 32.04° are attributed to the characteristic peaks of clinoptilolite [17, 24–27]. The XRD pattern of natural zeolite is typical of clinoptilolite with

Table 3 Bulk chemical compositions of natural and modified clinoptilolites

| Sample No	Constituent oxides, wt. %										Si/Al mol ratio
	SiO$_2$	Al$_2$O$_3$	Na$_2$O	K$_2$O	MgO	CaO	Fe$_2$O$_3$	TiO$_2$	MnO	LOI	
S0	61.90	12.20	0.76	2.45	1.38	3.73	1.89	0.22	0.07	15.40	4.31
S1	64.80	11.90	0.44	2.33	1.26	2.65	1.71	0.17	0.05	14.70	4.62
S2	64.20	11.80	–	2.32	1.18	2.78	1.83	0.12	0.04	14.70	4.62
S3	66.50	10.60	0.46	2.09	0.92	3.25	1.10	0.14	–	14.90	5.32
S4	72.50	8.48	0.32	1.90	0.62	1.26	1.52	0.20	–	13.10	7.25
S5	71.60	10.00	0.44	1.72	0.53	1.21	1.63	0.17	–	12.60	6.08
S6	72.30	6.34	0.55	1.50	–	3.67	0.91	–	–	14.70	9.68
S7	74.50	7.67	0.49	1.48	0.44	0.78	0.83	0.15	–	13.70	8.24
S8	72.40	8.64	0.58	1.49	0.70	0.89	1.63	0.15	–	13.50	7.11
S9	71.00	6.37	–	1.19	0.34	3.47	0.78	0.13	–	16.70	9.46
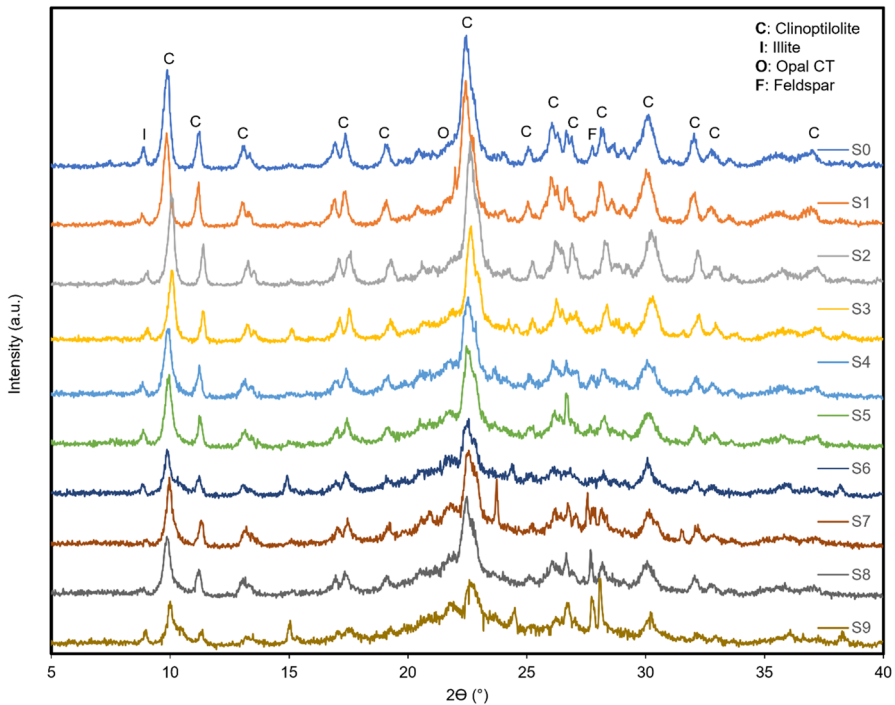
Fig. 1 XRD patterns of the natural and modified clinoptilolite samples

traces of impurities such as illite/mica ($2\theta = 8.8°$), feldspar ($2\theta = 27.7°$), and opal-cristobalite-tridymite (opal-CT) [17, 26–30]. The calcium oxalate formed by leaching calcium from natural clinoptilolite with an oxalic acid solution gave rise to diffraction peaks at 14.9° and 24.3° [31].

As shown in Fig. 1, the decrease in peak intensities with increasing acid concentration implies the partial destruction of the microstructure in the clinoptilolite owing to the removal of Al from the framework, which depends on the acid treatment parameters given in Table 1. The XRD peaks shifting to higher 2θ values can be explained by dealumination [32]. The oxalic acid treatment caused the highest shift in the XRD peaks of the samples (Fig. 1). While dealumination with mineral acids, such as HCl and HNO_3, shows poor performance in Al extraction, oxalic acid, which is an organic acid, is more efficient than mineral acids. The literature is consistent with these findings [33–35]. Additionally, the XRF data given in Table 3 show that the dealumination of natural clinoptilolite with acid treatment increases the Si/Al ratio.

The XRF and XRD results show that the acid treatments of the natural zeolite cause significant decationization and dealumination, resulting in a loss of crystallinity. From the XRD patterns, the main clinoptilolite peaks, e.g., (020), (200), and (330) for modified zeolites decrease with increasing the severity of acid treatment affected by the combined influences of acid concentration, treatment time, and temperature, which suggests the reduction of crystallinity of clinoptilolite.

The N$_2$ adsorption/desorption isotherms of the natural and modified clinoptilolites that are treated with 0.1 M-1.0 M different types of acid solutions are given in Figs. 2, 3, 4.

Natural clinoptilolite (S0) and acid-treated clinoptilolite samples (S1–S9) exhibit nitrogen sorption data consistent with hybrid type II/IVa isotherms [36]. Capillary condensation occurring in the mesopore structure together with hysteresis loops can be seen in the isotherms for the samples treated with various solutions under the parameters listed in Table 2 [36]. The pore size distributions of the natural and modified clinoptilolite samples were obtained using the NLDFT cylindrical pore model. The fitting errors between the experimental N$_2$ adsorption isotherms and the calculated isotherms of the natural and modified clinoptilolites were in the range of 0.35–0.92%. Depending on the acid treatment conditions, the cumulative pore volume curves and pore size distributions of the modified clinoptilolites are shown in Figs. 2b, 3b, 4b and Figs. 2c, 3c, 4c, respectively. S3, S4, S5, S7, S8, and S9 had
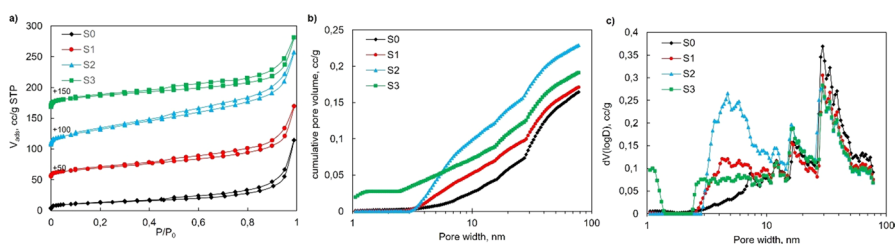
Fig. 2 **a** N$_2$ adsorption/desorption isotherms, **b** cumulative pore volume, and **c** pore size distribution of natural clinoptilolite (S0) and clinoptilolite samples treated with 0.1 M acid solutions (S1–S3)
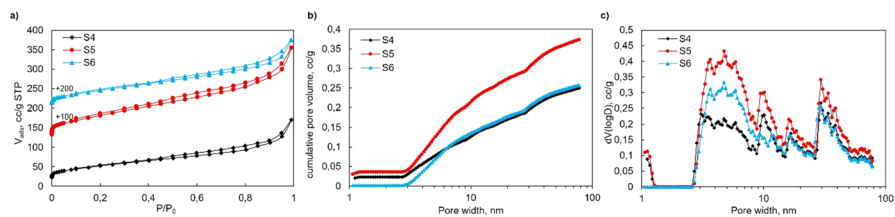

Fig. 3 **a** N$_2$ adsorption/desorption isotherms, **b** cumulative pore volume, and **c** pore size distribution of clinoptilolite samples treated with 0.5 M acid solutions (S4–S6)
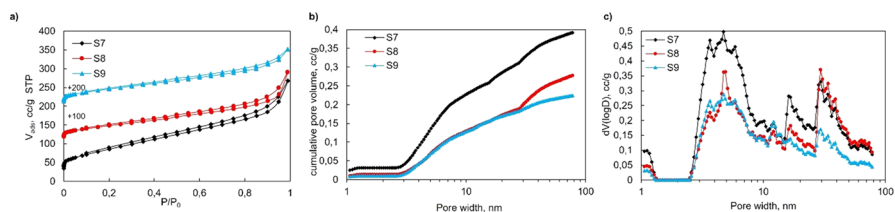

Fig. 4 **a** N$_2$ adsorption/desorption isotherms, **b** cumulative pore volume, and **c** pore size distribution of clinoptilolite samples treated with 1.0 M acid solutions (S7–S9)

micropores centered at 1.114 nm. Mesopores larger than 2.5 nm are more prominent than micropores for all modified clinoptilolites when the acid concentration and treatment temperature are increased. Zelenka stated that the filling of the finer micropores (diameter ≤ 1 nm) is associated with the slowest transport rate due to the molecular size of N_2 [37]. When the pore structure of clinoptilolite crystals is considered, the accessibility of N_2 molecules through the finer micropores of clinoptilolite might be difficult [24]. Therefore, the BET surface area (46.20 m^2/g) and pore volume (0.177 cc/g) of the S0 sample are relatively low. The data obtained from the N_2 adsorption isotherms are listed in Table 4. The BET surface areas and pore volumes of the modified clinoptilolites (S1-S9) are greater than those of the natural clinoptilolite (S0), and the BET surface area of the S7 sample reached 309.26 m^2/g with 0.414 cc/g pore volume after the acid treatment of the S0 sample with 1 M HCl at 80 °C for 3 h. These data suggest that acid treatment changes the textural properties of natural clinoptilolite, which increases its specific surface area and pore volume. These results are in good agreement with the literature findings [11, 26, 33, 34].

The NH_3-TPD profiles in Fig. A.1 were used to determine the acidic characteristics of natural and modified clinoptilolites. The samples contain weak and strong acid sites, as indicated by the NH_3-TPD results. The high-temperature peak (> 300 °C) is attributed to the strong acid sites that are typically assigned to the framework tetrahedral aluminum species, whereas the low-temperature peak (appearing below 300 °C) corresponds to the weak acid sites that are attributed to silanol groups or extra-framework aluminum species [38]. The dehydroxylation of the zeolitic material reported by Katranas et al. [39] matches the peak obtained for natural clinoptilolite above 625 °C. The number of weak acid sites decreased and the number of strong acid sites increased as the Si/Al ratio and metal ions in the natural clinoptilolite changed under various acid treatment conditions. The decrease in weak acid sites for the modified clinoptilolite suggests that extra-framework aluminum

Table 4 N_2 adsorption data for the natural and modified clinoptilolites

Sample	S_{BET} (m^2/g)	V_{micro}[a] (cc/g)	V_{total}[b] (cc/g)	Average pore size (nm)
S0	46	0.00209	0.177	15.32
S1	72	0.000631	0.185	10.34
S2	123	0	0.243	7.92
S3	131	0.0273	0.203	6.20
S4	186	0.0228	0.264	5.67
S5	291	0.0366	0.394	5.41
S6	170	0.00186	0.271	6.38
S7	309	0.0315	0.414	5.36
S8	174	0.0136	0.296	6.80
S9	167	0.0102	0.235	5.63

[a]DFT cumulative pore volume of pores with diameters below 2.0 nm
[b]Volume adsorbed at $p/p_0 = 0.99$

is removed when the natural zeolites are acid-modified [40]. The number of strong acid sites increased for all modified zeolites because decationization resulted in the reappearance of structural hydroxyls blocked by exchangeable cations [41]. Additionally, the displacement of cations forms acidic sites, and the number of cations depends on the amount of aluminum in the lattice [42]. The peak positions in the TPD profiles also provided information on the relative acid strength of the samples. The quantity of weak and strong acid sites was determined by integrating the area under each peak, as shown in Fig. A.1, and the results are presented in Table 5. Two desorption peaks were observed above 400 °C when the NH_3-TPD profiles of samples S3, S6, and S9 (Figure A.2) were analyzed. Even though these peaks were predicted to be strong acid sites, it was found that the peaks were caused by the thermal decomposition of calcium oxalate when the XRD patterns of the same samples were investigated. According to Hourlier [43], these peaks are the result of calcium oxalate decomposition, which begins between 443 °C and 550 °C and above 580 °C following the oxalic acid treatment of the S0 sample. As a result, the peaks in the S3, S6, and S9 samples were not considered or calculated as acidic sites.

Hydrogen adsorption of clinoptilolite samples

The hydrogen adsorption measurements were carried out at liquid nitrogen temperature up to a pressure of 1.0 bar. The H_2 adsorption isotherms of the natural clinoptilolite (S0) and acid-treated clinoptilolites (S1-S9) that are the average of 1st and 2nd trials are shown in Fig. 5.

Figure 5 demonstrates how the acid treatment enhanced the ability of natural clinoptilolite to adsorb hydrogen. The capacity of natural clinoptilolite for hydrogen adsorption was affected by the acid treatment settings listed in Table 2. Table 6 summarizes the modified clinoptilolites' hydrogen storage capacity at 1.0 bar as determined by the isotherms.

A statistical analysis of variance (ANOVA) was used to estimate the contribution of each parameter to the maximum hydrogen adsorption capacity of natural clinoptilolite at 77 K and 1.0 bar pressure. ANOVA allows a better understanding of the accuracy of the observed data and whether the tests were performed under controlled conditions [20, 21, 44]. The ANOVA results are listed in Table 7.

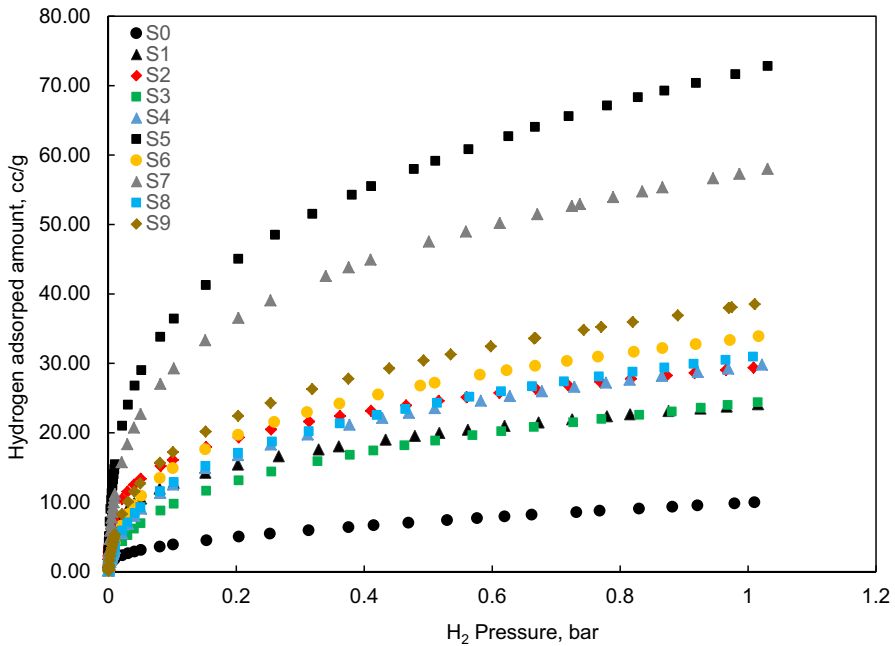| Table 5 Acidity derived from NH_3-TPD for natural and modified clinoptilolites	Sample	T_{max}	Weak acid sites (mmol/g)	T_{max}	Strong acid sites (mmol/g)	Total acid sites (mmol/g)
	S0	229	1.75	497	1.54	3.29
	S1	228	1.42	534	1.85	3.27
	S2	234	1.38	538	1.87	3.25
	S4	227	0.86	519	1.88	2.74
	S5	235	0.88	526	2.06	2.94
	S7	235	0.72	508	2.12	2.84
	S8	227	0.77	524	2.04	2.81

Fig. 5 Hydrogen adsorption isotherms of natural clinoptilolite (S0) and modified clinoptilolites (S1–S9) at 77 K

Table 6 The hydrogen adsorption capacities of the modified clinoptilolites at 77 K and 1.0 bar

Experiment no	Trial		
	1st (mmol/g)	2nd (mmol/g)	Average (mmol/g)
1	1.230	0.932	1.081
2	1.110	1.510	1.310
3	1.144	1.044	1.094
4	1.348	1.315	1.332
5	3.526	2.983	3.255
6	1.440	1.583	1.512
7	2.793	2.375	2.584
8	1.124	1.650	1.387
9	1.614	1.823	1.719

The F-value, given in Table 7, is the ratio of the mean square of the term to the mean square of the error, and a larger F-value indicates that the parameter is more significant [20, 21, 44]. The importance of the acid treatment parameters of natural clinoptilolite, which maximize the hydrogen adsorption capacity, was evaluated based on the F-values in Table 7. It can be deduced that the treatment temperature had the greatest impact, whereas the type of acid solution had the least impact. The significant order of acid treatment parameters on the natural clinoptilolite to

Table 7 Results of variance analysis for the experiments

Source	Degree of Freedom	Sum of squares	Mean square	F-value	p value
A: Concentration of solution, M	2	2.633	1.316	22.15	0.000
B: Type of solution	2	0.892	0.446	7.51	0.012
C: Temperature, °C	2	3.440	1.720	28.96	0.000
D: Time, h	2	1.774	0.887	14.93	0.001
Error	9	0.535	0.0594		
Total	17	9.274			

maximize the hydrogen adsorption capacity is treatment temperature > concentration of solution > treatment time > type of solution. The signal-to-noise ratios (S/N) of the experimental data were calculated using the Minitab 18 software. Larger-the-better performance characteristics were chosen to identify the optimum acid treatment conditions for natural clinoptilolite to maximize its hydrogen adsorption capacity. The main effects of each of the factors listed in Table 1 on hydrogen adsorption capacity are shown in Fig. 6.

When analyzing the signal-to-noise ratios presented in Fig. 6, to maximize the hydrogen absorption capacity, which is the performance characteristic, the highest signal-to-noise ratios obtained from the levels of the relevant parameters should be preferred. Thus, the solution should have a concentration of 0.5 M, be of solution type HNO_3, the treatment temperature should be 80 °C, and the treatment time
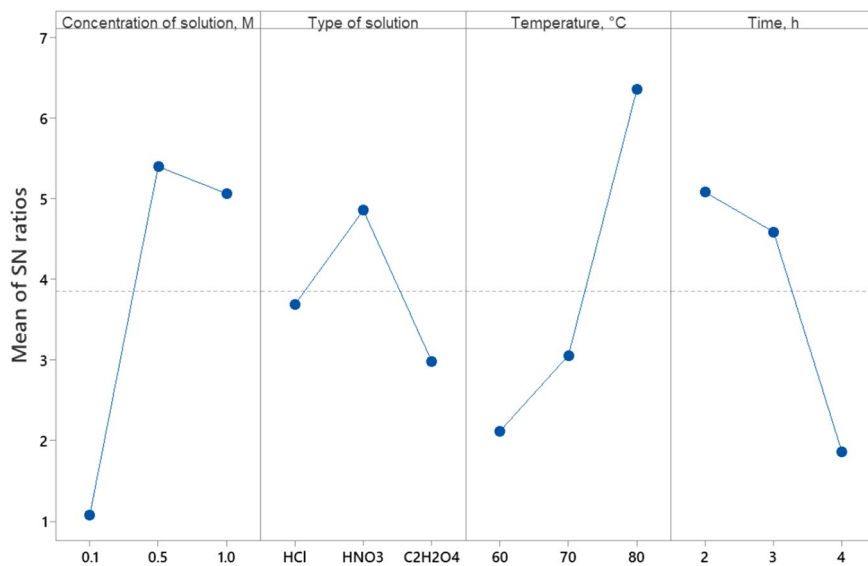
Fig. 6 Main effects of each factor on hydrogen absorption capacity

should be 2 h. When Table 2 is examined, it can be seen that these experimental conditions are the same as in experiment S5. There is no need to perform a verification experiment because the parameters and levels in the experimental plan (S5) that provide the optimal conditions for maximizing the hydrogen adsorption capacity of clinoptilolite are already known. A verification experiment was necessary for all the other cases. To explain why S5 shows a higher hydrogen adsorption capacity than the other samples, the textural properties of the clinoptilolite samples must be considered. Chung investigated the roles of the framework structure, surface area, and pore volume of zeolites on hydrogen adsorption and stated that the largest hydrogen storage was obtained on the ultra-stable Y zeolite because of its larger surface area and pore volume than the other zeolites [45]. It has also been reported that the amount of hydrogen adsorption on mordenite zeolites increases with increasing Si/Al molar ratio, which was achieved by dealumination [45]. Although the hydrogen adsorption capacity of the acid-treated samples (S1-S9) increased relative to that of natural clinoptilolite (S0) with increasing BET surface area, pore volume, and Si/Al molar ratio, the hydrogen adsorption capacity of the acid-treated samples was not always proportional to the properties of the clinoptilolite samples. For instance, although the BET surface area and total pore volume of the S7 sample (309.26 m^2/g; 0.41 cc/g) are comparatively greater than those of the S5 sample (291.34 m^2/g; 0.39 cc/g), the H$_2$ uptake of the S5 sample is higher than that of the S7 sample. According to Huang et al., pore size significantly affects H$_2$ storage performance, and nanopores smaller than 1.5 nm are the most effective hydrogen storage spaces, regardless of whether they are used at low or high pressures [46]. The S5 sample had the largest hydrogen uptake (3.255 mmol/g) compared to the modified samples, which is ascribed to the higher cumulative pore volume of the pores with a diameter below 1.5 nm (Table 4).

The hydrogen adsorption capacities of the modified zeolites are influenced by several factors, not just the fact that an efficient H$_2$ storage material has a large surface area and high micropore volume. This can be explained by evaluating the hydrogen adsorption capabilities of the S4 and S8 samples. The S8 has a better capacity for hydrogen adsorption than the S4, despite the S4 having a larger surface area and micropore volume (186.1 m^2/g; 0.0288 cc/g) than the S8 sample (174.05 m^2/g; 0.0136 cc/g). The NH$_3$-TPD data in Table 5 demonstrate that despite the almost equal number of strong acid sites in the S4 and S8 samples, the S8 sample's strong acid desorption peak shifted to a higher temperature, indicating that the S8 sample's strong acid is stronger than that of S4 sample's. S8 shows a higher capacity for hydrogen adsorption than S4, which can be attributed to its stronger acid sites. S1 and S2 exhibit the same features. Therefore, a material made from natural zeolite that can effectively store hydrogen needs to have a large surface area, a multitude of micropores, and strong acid sites.

Adsorption isotherm

The amount of gas adsorbed on a solid at different pressures but constant temperature is shown by the adsorption isotherms [47]. The modeling of adsorption

isotherm data is significant for the design of adsorption systems and for comparing the adsorption performance of adsorbents [48]. Although many adsorption isotherm models are available in the literature [49, 50], well-known adsorption isotherm models, namely Langmuir and Freundlich, have been applied to describe the equilibrium relationships between hydrogen gas and natural clinoptilolite samples.

While the Langmuir isotherm model assumes monolayer adsorption on a homogeneous surface [48], the Freundlich model is not restricted to monolayer formation and is applicable to gas-phase systems with heterogeneous surfaces [50]. The Langmuir and Freundlich isotherm equations are expressed as follows [50, 51]:

$$\text{Langmuir equation}: \quad q = \frac{q_m K_L P}{1 + K_L P} \tag{1}$$

$$\text{Freundlich equation}: \quad q = K_F P^{1/n} \tag{2}$$

where q is the amount of H_2 adsorbed on a clinoptilolite sample (mmol/g), P is the H_2 pressure (bar), q_m (mmol/g) and K_L(1/bar) are the Langmuir isotherm constants, K_F (mmol/g. bar$^{1/n}$), and n is the Freundlich isotherm constant. The constants were determined by nonlinear regression analysis using Polymath 6.10 software, and the results at 95% confidence intervals are given in Table 8.

Table 8 shows that the degree of interaction between the hydrogen gas and S5 sample is stronger than that of S0 sample because the K_L and K_F values of S5 are larger than those of S0. Al-Hajjaj et al. stated that higher values of K_L indicate a stronger degree of interaction between the gas and solid surface [49]. The value of (1/n) calculated using the Freundlich isotherm model is the intensity of the adsorption or surface heterogeneity, which indicates the relative energy distribution and heterogeneity of the adsorbate sites [50]. Adsorption is favorable when the (1/n) value is between 0 and 1 [50]. In this study, the (1/n) values of S0 and S5 were 0.385 and 0.338, respectively. Therefore, the adsorption process was favorable at the liquid nitrogen temperature. A comparison between the experimental and model data for hydrogen adsorption of the S0 and S5 samples at 77 K is shown in Fig. 7.

Figure 7 indicates that the Freundlich isotherm model is in good agreement with the experimental data, which is also evident from the correlation coefficient (R^2) in Table 8.

The H_2 adsorption capacity of S5 was compared with that of porous materials such as natural zeolites and clay minerals at 77 K and 1.0 bar. The results are summarized in Table 9.

Table 8 Adsorption isotherm constants for S0 and S5 samples at 77 K

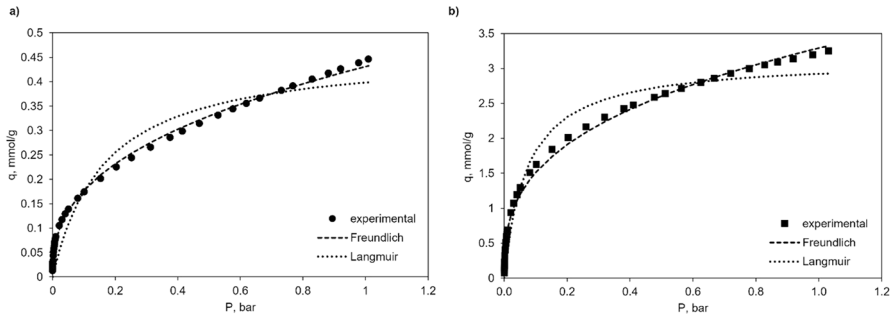| Samples	Langmuir			Freundlich		
	q_m (mmol/g)	K_L (1/bar)	R^2	K_F (mmol/g bar$^{1/n}$)	n	R^2
S0	0.463	6.155	0.948	0.431	2.598	0.998
S5	3.133	13.890 ± 0.008	0.966	3.292 ± 0.047	2.958 ± 0.095	0.996

Fig. 7 Comparison between the experimental and model data for hydrogen adsorption in (a) S0 and (b) S5 at 77 K

Table 9 A comparison of the H_2 adsorption capacities of various adsorbents at 77 K and 1.0 bar

Adsorbent type	H_2 adsorption capacity (mmol/g)	References
S5 (Natural clinoptilolite was treated with 0.5 M HNO_3 at 80 °C for 2 h)	3.255	This study
CLN-2N (Clinoptilolite-rich tuff was treated with 2 M HNO_3 at 90 °C for 4 h)	2.391	[18]
Li-Clinoptilolite	2.752	[17]
Li-Mordenite	1.670	[17]
M-3N (Mordenite-rich tuff was treated with 3 M HNO_3 at 80 °C for 3 h)	1.672	[52]
SH-05 (Sepiolite was treated with 0.5 M H_2SO_4 at 80 °C for 5 h)	2.252	[53]
BH-4 (Bentonite was treated with 4 M H_2SO_4 at 80 °C for 5 h)	1.003	[53]

Table 9 shows that the hydrogen adsorption capacity of S5 was significantly greater than that of the other samples. Natural zeolites consist of different types of naturally occurring cations whose quantities and proportions vary with the location of the mineral deposits. The accompanying minerals, amorphous SiO_2 structure, and presence of cations in the micropore structure block the pores of natural zeolite [54]. The Si/Al ratio and textural characteristics of natural zeolites, such as the specific surface area and micropore volume, depend on acid treatment conditions [11]. Therefore, acid treatment conditions should be optimized to increase the hydrogen adsorption capacity of natural clinoptilolite. As a result, natural clinoptilolite treated with 0.5 M HNO_3 at 80 °C for 2 h can be considered a promising adsorbent for hydrogen adsorption.

Conclusions

Optimization of the acid treatment parameters is extremely important for the preparation of natural clinoptilolite as a H_2 storage material. In this study, an L9 orthogonal array of the Taguchi method was applied to investigate the influence of acid treatment parameters, namely concentration of a solution, type of acid solution (inorganic and organic acid), treatment temperature, and treatment time, on the hydrogen adsorption capacity of the natural clinoptilolite. After evaluating the variance analysis results, it is evident that the temperature parameter has the highest F-value, followed by solution concentration, treatment time, and type of solution. Based on these findings, temperature is the most effective parameter in clinoptilolite modification for maximizing H_2 absorption, and the least effective parameter is the type of solution. This is supported by the p values, and it is stated that the experiments are within the 95% confidence interval. The results showed that the acid treatment conditions affected the specific surface area, pore volume, and pore size, as well as the acidic sites of natural clinoptilolite; the S5 sample, in which S0 was treated with 0.5 M HNO_3 at 80 °C for 2 h, had the highest hydrogen adsorption capacity relative to the untreated clinoptilolite (S0). Additionally, the hydrogen adsorption isotherms of samples S0 and S5 can be expressed using the Freundlich isotherm model.

Appendix

See Figs. 8, 9.
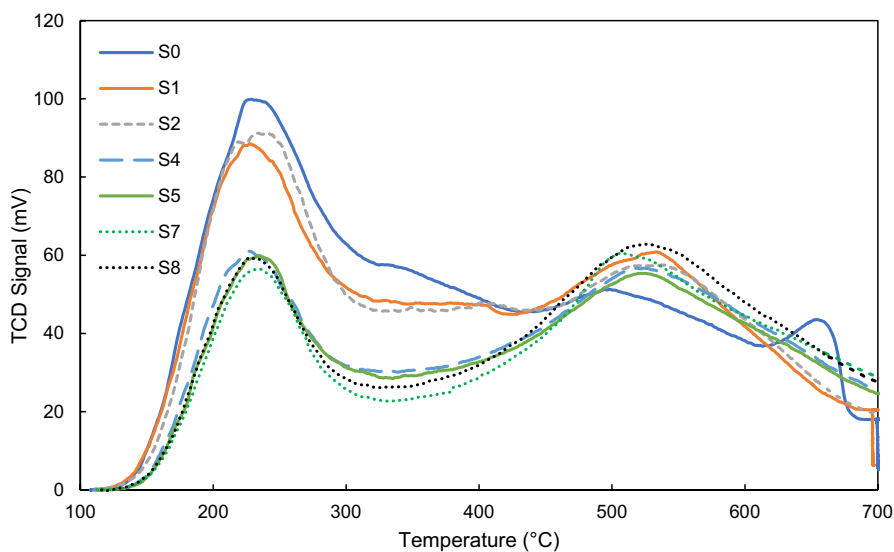
Fig. 8 NH₃-TPD profiles of the natural and modified clinoptilolite samples
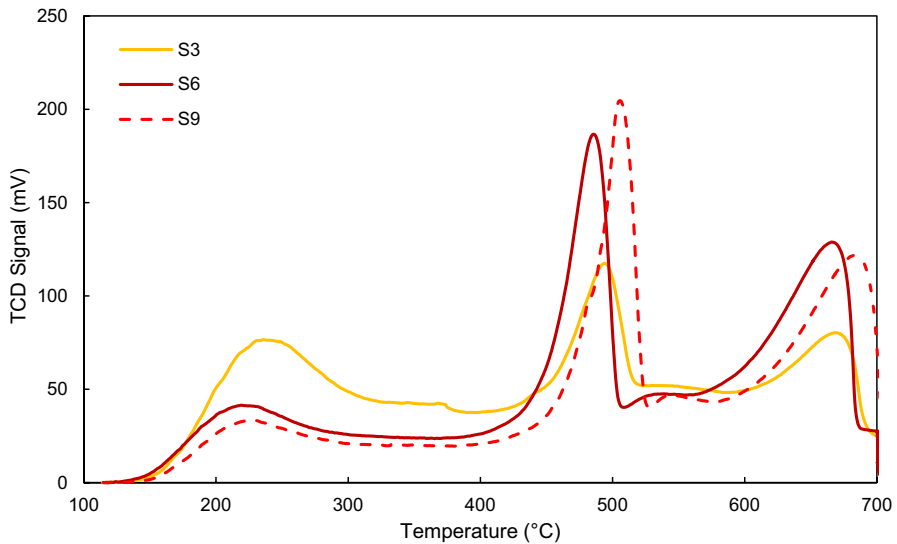
Fig. 9 NH$_3$-TPD profiles of the S3, S6, and S9 samples

Declarations

Competing interests I declare that the authors have no competing interests as defined by Springer or other interests that might be perceived to influence the results and/or discussion reported in this manuscript.

Ethical approval This declaration is not relevant to the content of our submission, and it is not applicable.

References

1. P. Jaramillo, S. Kahn Ribeiro, P. Newman, S. Dhar, O. E. Diemuodeke, T. Kajino, D. S. Lee, S. B. Nugroho, X. Ou, A. Hammer Strømman, and J. Whitehead, *2022: Transport. In IPCC, 2022: Climate Change 2022: Mitigation of Climate Change. Contribution of Working Group III to the Sixth Assessment Report of the Intergovernmental Panel on Climate Change [P.R. Shukla, J. Skea, R. Slade, A. Al Khourdajie, R. van Diemen, D. McCollum, M. Pathak, S. Some, P. Vyas, R. Fradera, M. Belkacemi, A. Hasija, G. Lisboa, S. Luz, J. Malley, (Eds.)].* (Cambridge, UK and New York, NY, USA., 2022)
2. S. Dhakal, J. C. Minx, F. L. Toth, A. Abdel-Aziz, M. J. Figueroa Meza, K. Hubacek, I. G. C. Jonckheere, Yong-Gun Kim, G. F. Nemet, S. Pachauri, X. C. Tan, and T. Wiedmann, *2022: Emissions Trends and Drivers. In IPCC, 2022: Climate Change 2022: Mitigation of Climate Change. Contribution of Working Group III to the Sixth Assessment Report of the Intergovernmental Panel on Climate Change [P.R. Shukla, J. Skea, R. Slade, A. Al Khourdajie, R. van Diemen, D. McCollum, M. Pathak, S. Some, P. Vyas, R. Fradera, M. Belkacemi, A. Hasija, G. Lisboa, S. Luz, J. Malley, (Eds.)].* (2022)
3. B. McNicol, D.A.J. Rand, K.R. Williams, J. Power. Sources **100**, 47 (2001)
4. T. Capurso, M. Stefanizzi, M. Torresi, S.M. Camporeale, Energy Convers. Manag. **251**, 114898 (2022)
5. E.B. Agyekum, C. Nutakor, A.M. Agwa, S. Kamel, Membranes (Basel) **12**, 173 (2022)
6. Y. Manoharan, S.E. Hosseini, B. Butler, H. Alzhahrani, B.T.F. Senior, T. Ashuri, J. Krohn, Appl. Sci. **9**, 2296 (2019)
7. A. Ajanovic, M. Sayer, R. Haas, Int. J. Hydrog. Energy **47**, 24136 (2022)
8. H. W. Langmi, N. Engelbrecht, P. M. Modisha, and D. Bessarabov, in *Electrochemical Power Sources: Fundamentals, Systems, and Applications Hydrogen Production by Water Electrolysis* (Elsevier, 2021), pp. 455–486
9. S.-Y. Lee, J.-H. Lee, Y.-H. Kim, J.-W. Kim, K.-J. Lee, S.-J. Park, Processes **10**, 304 (2022)
10. J. Dong, X. Wang, H. Xu, Q. Zhao, J. Li, Int. J. Hydrog. Energy **32**, 4998 (2007)
11. C. Wang, S. Leng, H. Guo, J. Yu, W. Li, L. Cao, J. Huang, Appl. Surf. Sci. **498**, 143874 (2019)
12. D.A. Kennedy, F.H. Tezel, Microporous Mesoporous Mater. **262**, 235 (2018)
13. W. An, P. Swenson, A. Gupta, L. Wu, T.M. Kuznicki, S.M. Kuznicki, J. Membr. Sci. **433**, 25 (2013)
14. N. Mansouri, N. Rikhtegar, H. Ahmad Panahi, F. Atabi, and B. K. Shahraki, Environment Protection Engineering **39**, 139 (2013)
15. M.W. Ackley, R.T. Yang, AIChE J. **37**, 1645 (1991)
16. M.W. Ackley, R.F. Giese, R.T. Yang, Zeolites **12**, 780 (1992)
17. B. Erdoğan Alver and M. Sakızcı, Int. J. Hydrog. Energy **44**, 6748 (2019)
18. B. Erdoğan, G. Dikmen, Int. J. Hydrog. Energy **45**, 2017 (2020)
19. C. Wang, H. Guo, S. Leng, J. Yu, K. Feng, L. Cao, J. Huang, Crit. Rev. Solid State Mater. Sci. **46**, 330 (2021)
20. R. K. Roy, *Design of Experiments Using The Taguchi Approach: 16 Steps to Product and Process Improvement*, 1st ed. (Wiley-Interscience, 2001)
21. R.K. Roy, *A Primer on the Taguchi Method*, 1st edn. (Society of Manufacturing Engineers, Dearborn, MI, 1990)
22. P.J. Ross, *Taguchi Techniques for Quality Engineering: Loss Function, Orthogonal Experiments, Parameter and Tolerance Design* (McGraw-Hill, New York, 1988)
23. K.A. Cychosz, R. Guillet-Nicolas, J. García-Martínez, M. Thommes, Chem. Soc. Rev. **46**, 389 (2017)
24. T. S. Diógenes, R. G. Santiago, D. A. S. Maia, D. v. Gonçalves, D. C. S. Azevedo, S. M. P. Lucena, and M. Bastos-Neto, Chem. Eng. Res. Des. **177**, 640 (2022)
25. G. Narin, D. Balköse, S. Ülkü, Drying Technol. **29**, 553 (2011)
26. B. Erdoğan Alver, J Hazard Mater **262**, 627 (2013)
27. N. Mortazavi, M. Bahadori, A. Marandi, S. Tangestaninejad, M. Moghadam, V. Mirkhani, I. Mohammadpoor-Baltork, Sustain. Chem. Pharm. **22**, 100495 (2021)
28. S. Nowak, S. Lafon, S. Caquineau, E. Journet, B. Laurent, Talanta **186**, 133 (2018)
29. J.M. Elzea, S.B. Rice, Clays Clay Miner. **44**, 492 (1996)
30. M. Hernández-Ortiz, G. Hernández-Padrón, R. Bernal, C. Cruz-Vázquez, V. Castano, Int. J. Basic Appl. Sci. **4**, 238 (2015)

31. Z. Tišler, K. Hrachovcová, E. Svobodová, J. Šafář, L. Pelíšková, Minerals **9**, 719 (2019)
32. R. Putra, W.W. Lestari, B.H. Susanto, G.T.M. Kadja, Energy Sources Part A: Recov. Util. Environ. Eff. **44**, 7483 (2022)
33. C.F. Imbachi-Gamba, A.L. Villa, Mater. Today Chem. **20**, 100442 (2021)
34. R. Giudici, H.W. Kouwenhoven, R. Prins, Appl. Catal. A Gen. **203**, 101 (2000)
35. R. Zhang, D. Raja, Y. Zhang, Y. Yan, A.A. Garforth, Y. Jiao, X. Fan, Top. Catal. **63**, 340 (2020)
36. M. Thommes, K. Kaneko, A. V. Neimark, J. P. Olivier, F. Rodriguez-Reinoso, J. Rouquerol, and K. S. W. Sing, Pure Appl. Chem. **87**, 1051 (2015)
37. T. Zelenka, Microporous Mesoporous Mater. **227**, 202 (2016)
38. Q. Wang, Z.-M. Cui, C.-Y. Cao, W.-G. Song, J. Phys. Chem. C **115**, 24987 (2011)
39. T.K. Katranas, A.G. Vlessidis, V.A. Tsiatouras, K.S. Triantafyllidis, N.P. Evmiridis, Microporous Mesoporous Mater. **61**, 189 (2003)
40. J. Li, L. Wang, D. Zhang, J. Qian, L. Liu, J. Xing, J. Fuel Chem. Technol. **47**, 957 (2019)
41. A. Ates, C. Hardacre, J. Colloid Interface Sci. **372**, 130 (2012)
42. H. Karami, M. Kazemeini, S. Soltanali, M. Rashidzadeh, Can. J. Chem. Eng. **100**, 3357 (2022)
43. D. Hourlier, J. Therm. Anal. Calorim. **136**, 2221 (2019)
44. M.S. Phadke, *Quality Engineering Using Robust Design* (Prentice Hall, Englewood Cliffs, NJ, 1989)
45. K.-H. Chung, Energy **35**, 2235 (2010)
46. J. Huang, Y. Liang, H. Dong, H. Hu, P. Yu, L. Peng, M. Zheng, Y. Xiao, Y. Liu, Int. J. Hydrog. Energy **43**, 18077 (2018)
47. S.H. Fogler, *Elements of Chemical Reaction Engineering*, 3rd edn. (Prentice-Hall, Englewood Cliffs, NJ, 1998)
48. M.I. El-Khaiary, J. Hazard. Mater. **158**, 73 (2008)
49. A. Al-Hajjaj, B. Zamora, A.A. Shah, E. Reguera, D.V. Bavykin, F.C. Walsh, Int. J. Hydrog. Energy **36**, 14464 (2011)
50. M. A. Al-Ghouti and D. A. Da'ana, J Hazard Mater **393**, 122383 (2020)
51. D. Saha, Z. Wei, S. Deng, Int. J. Hydrog. Energy **33**, 7479 (2008)
52. B. Erdoğan Alver and F. Esenli, Microporous and Mesoporous Mater. **244**, 67 (2017)
53. B. Erdoğan Alver, Int. J. Hydrog. Energy **43**, 831 (2018)
54. Z. Tisler, J. Horacek, J. Safar, R. Velvarska, L. Peliskova, J. Kocik, Y. Gherib, K. Marklova, R. Bulanek, D. Kubicka, Microporous Mesoporous Mater. **282**, 169 (2019)